MOLECULAR IMAGING

Chemical exchange saturation transfer MR imaging of Parkinson's disease at 3 Tesla

Chunmei Li · Shuai Peng · Rui Wang · Haibo Chen · Wen Su · Xuna Zhao · Jinyuan Zhou · Min Chen

Abstract

Objectives To demonstrate the feasibility of using chemical exchange saturation transfer (CEST) imaging to detect Parkinson's disease (PD) in patients at 3 Tesla.

Methods Twenty-seven PD patients (17 men and 10 women; age range, 54–77 years) and 22 age-matched normal controls (13 men and 9 women; age range, 55–73 years) were examined on a 3-Tesla MRI system. Magnetization transfer spectra with 31 different frequency offsets (−6 to 6 ppm) were acquired at two transverse slices of the head, including the basal ganglia and midbrain. One-way analysis of variance tests was used to compare the differences in CEST imaging signals between PD patients and normal controls.

Results Total CEST signal between the offsets of 0 and 4 ppm in the substantia nigra was significantly lower in PD patients than in normal controls ($P=0.006$), which could be associated with the loss of dopaminergic neurons. Protein-based CEST imaging signals at the offset of 3.5 ppm in the globus pallidus, putamen and caudate were significantly increased in PD patients, compared to normal controls ($P<0.001$, $P=0.003$, $P<0.001$, respectively).

Conclusions CEST imaging signals could potentially serve as imaging biomarkers to aid in the non-invasive molecular diagnosis of PD.

Key Points
- *Total CEST signal in substantia nigra decreased in PD patients*
- *Protein-based CEST signals in basal ganglia increased in PD patients*
- *CEST could assist with the non-invasive molecular diagnosis for PD patients*

Abbreviations

APT	amide proton transfer
CEST	chemical exchange saturation transfer
FLAIR	fluid-attenuated inversion recovery
H&Y	Hoehn and Yahr
MTR_{asym}	magnetization transfer ratio asymmetry
NAWM	normal-appearing white matter
PD	Parkinson's disease

C. Li · S. Peng · R. Wang · M. Chen (✉)
Department of Radiology, Beijing Hospital, No. 1 Da-Hua Road, Dong Dan, Beijing 100730, China
e-mail: chenmin62@yahoo.com

H. Chen · W. Su
Department of Neurology, Beijing Hospital, No. 1 Da-Hua Road, Dong Dan, Beijing 100730, China

X. Zhao
Center for MRI Research and Beijing City Key Lab for Medical Physics & Engineering, Peking University, No.5 Yiheyuan Road, Haidian District, Beijing 100871, China

J. Zhou (✉)
Department of Radiology, Johns Hopkins University, 600 N. Wolfe Street / Park 336, Baltimore, MD 21287, USA
e-mail: jzhou@mri.jhu.edu

Introduction

Parkinson's disease (PD) is a neurodegenerative disease, characterized by degenerative changes in the dopaminergic neurons in the substantia nigra that result in a decreased dopamine level [1]. Currently, the diagnosis of PD is based primarily on the clinical manifestations. Unfortunately, clinicopathologic studies have revealed substantial error rates for the clinical diagnosis of PD (up to 25 %) even for experienced neurologists [2, 3]. Imaging biomarkers in different modalities, such

as MRI and PET, for both risk and disease progression are crucial to our understanding of the disease and the development of new therapies [4–6]. Conventional MRI does not show specific changes in PD. The use of advanced MRI techniques, such as diffusion imaging [7–9], susceptibility-weighted imaging [10, 11] and magnetization transfer imaging [12–14], may increase the accuracy of PD diagnosis. However, none of these methods have been regarded as a gold standard in the diagnosis of PD to date.

Chemical exchange saturation transfer (CEST) imaging has recently emerged as an important contrast mechanism for MRI in the field of molecular imaging [15, 16]. Currently, the CEST approach has several promising applications, including amide proton transfer (APT) for mobile proteins and peptides in tissue (such as those in the cytoplasm) [17, 18] (unlike the traditional magnetization transfer imaging method that is sensitive to solid-like proteins in tissue [19, 20]), gluCEST for glutamates [21, 22], glucoCEST for glucoses [23, 24], and many others [25, 26]. Of these CEST techniques, APT imaging works well with standard clinical 3-T MRI. It has been demonstrated previously that APT imaging is able to identify the spatial extent and pathological grade of several kinds of tumours [27–29] due to increased mobile protein and peptide content, and detect tissue pH changes in stroke (where pH decreases) [30, 31]. However, no study has been published about using CEST imaging on PD patients, and whether CEST imaging can provide unique information about PD is still unknown.

The purpose of this study was to test the feasibility of CEST imaging of PD patients at 3 Tesla, and to assess whether the CEST signal has potential for the evaluation of PD. Previous studies [1] have confirmed that substantia nigra is the first region involved in PD, followed by striatum. Therefore, we focused on these two brain regions in this study. We hypothesize that the loss of dopaminergic neurons in the substantia nigra of PD [32, 33] is associated with low CEST-MRI signal, while the accumulation of abnormal cytoplasmic proteins (such as α-synuclein) in some other areas (such as striatum) [34, 35] is associated with high APT-MRI signal.

Materials and methods

Subjects

This study was approved by the local institutional review board. All subjects gave written, informed consent prior to participation in this study. Twenty-seven PD patients (17 men and 10 women; mean age, 61.0 years; range, 54–77 years; 10.5±3.2 years of education) and 22 age- and education-matched normal controls (13 men and nine women; mean age, 59.2 years; 12.6±2.9 years of education) were recruited for this study.

The inclusion criteria for the PD group were as follows: hypokinesia; muscle rigidity; static tremor; unilateral onset and a positive response to dopaminergic drugs. Experienced neurologists ultimately diagnosed all the patients. Subjects were assessed with the Hoehn and Yahr (H&Y) scale and the unified Parkinson's disease rating scale while off all medications. The 27 PD patients were categorized as H&Y stage 1, $n=3$; stage 1.5, $n=4$; stage 2, $n=7$; stage 2.5, $n=7$; stage 3, $n=4$; and stage 4, $n=2$. They were asked to take no medications during the 12 h before the MR examination.

For both the PD patients and normal controls, exclusion criteria were as follows: a history of stroke; head trauma; exposure to anti-dopaminergic drugs; central nervous system infection; or other neurologic or psychiatric diseases and a structural lesion or hydrocephalus on brain magnetic resonance images.

MRI protocol

All PD patients and normal controls were imaged on a 3-Tesla MRI system (Achieva 3.0 T; Philips Medical Systems, Best, the Netherlands), using a dual-channel body coil for transmission and an eight-channel sensitivity-encoding coil for reception. Pencil beam second-order shimming was employed. Prior to APT imaging, routine images, including axial T2-weighted, T1-weighted and fluid-attenuated inversion recovery (FLAIR), were acquired to confirm that there was no structural abnormality.

CEST/APT imaging was based on a single-shot, turbo-spin-echo readout: repetition time, 3,000 ms; turbo-spin-echo factor, 54; field of view, 230 mm×221 mm; matrix, 105×100 (reconstructed to be 400×400); slice thickness, 6 mm. Two transverse slices of the head, including the basal ganglia and midbrain, were acquired. We used a pseudo-continuous wave radio frequency (RF) irradiation (saturation duration, 200 ms×4; inter-pulse delay, 10 ms; power level, 2 µT) and a multi-offset, multi-acquisition CEST/APT imaging protocol [36]. The 31 offsets were 0, ±0.25, ±0.5, ±0.75, ±1 ($n=2$), ±1.5 ($n=2$), ±2 ($n=2$), ±2.5 ($n=2$), ±3 ($n=2$), ±3.25 ($n=2$), ±3.5 ($n=8$), ±3.75 ($n=2$), ±4 ($n=2$), ±4.5, ±5, ±6 ppm (the values in parentheses are the number of acquisitions, which is 1 if not specified). An unsaturated image was acquired for the signal normalization. The saturated image at 15.6 ppm was also acquired to calculate the MTR value relating to conventional magnetization transfer imaging. The acquisition time was about 3 min per slice.

Data processing

The image analysis was performed using the Interactive Data Language (IDL, ITT Visual Information Solutions, Boulder, CO, USA). The measured magnetization transfer spectra (S_{sat}/S_0, in which S_{sat} and S_0 are the signal intensities with and

without selective RF irradiation, respectively, plotted as a function of saturation frequency offset, relative to water) were corrected for B_0 field heterogeneity effects on a pixel-by-pixel basis. CEST/APT imaging was quantified through the magnetization transfer ratio (MTR=$1-S_{sat}/S_0$) asymmetry (MTR$_{asym}$) analysis with respect to the water resonance. The calculated MTR$_{asym}$(3.5 ppm) images were called APT-weighted images [37, 38]. We further defined the total CEST signal intensity, MTR$_{asym}^{total}$, as the integral of the MTR$_{asym}$ spectrum in the range of 0 to 4 ppm.

The quantitative image analysis and comparison between PD patients and normal controls were performed by two radiologists (CL and RW, who had 5 and 10 years of experience in brain imaging, respectively). The FLAIR image was used as the anatomical reference to draw regions of interest (substantia nigra, red nucleus, globus pallidus, putamen and caudate of both hemispheres), as shown in Fig. 1. Besides, the normal-appearing white matter (NAWM) of the frontal lobe in the basal ganglia and the NAWM of the occipital lobe in the midbrain were assessed to determine whether changes in CEST signals existed between PD patients and normal controls.

Statistical analysis

All data were analysed using the statistical package SPSS16.0. The average CEST/APT imaging intensities [MTR$_{asym}$(3.5 ppm), MTR$_{asym}^{total}$ and MTR(15.6 ppm)] and corresponding 95 % confidence intervals were calculated for each region. A one-way analysis of variance test, followed by the Tukey test, was used to compare the differences in MTR$_{asym}$(3.5 ppm), MTR$_{asym}^{total}$ and MTR(15.6 ppm) for PD patients and normal controls, as well as

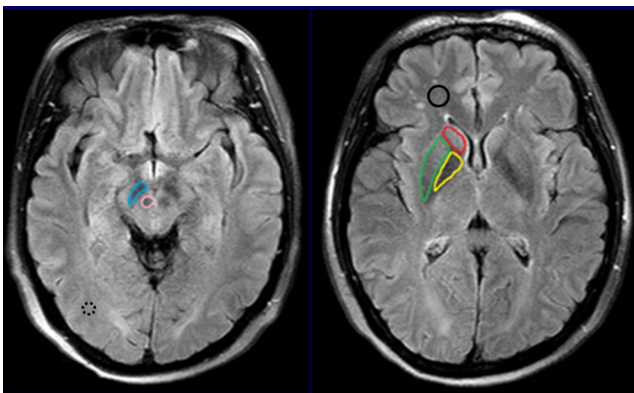
Fig. 1 Examples of the definition of the regions of interest for quantitative analysis. MTR$_{asym}$(3.5 ppm), MTR$_{asym}^{total}$ and MTR(15.6 ppm) were measured for each region. The values of each side were recorded as separate samples. The median voxel numbers of the substantia nigra (*blue*), red nucleus (*pink*), globus pallidus (*yellow*), putamen (*green*) and caudate (*red*) were 84 (range, 64–101), 61 (range, 49–80), 165 (range, 130–197), 211 (range, 165–240) and 105 (range, 80–138), respectively. The median voxel numbers of the frontal NAWM (*solid black*) and the occipital NAWM (*dashed black*) were 167 (range, 133–198) and 75 (range, 62–91), respectively

at different stages (early stage i.e. H&Y stages 1–2 vs. advanced stage i.e. H&Y stages ≥2.5). The level of significance was set at $P<0.05$.

Results

Detection of PD

Figure 2a–e compares the average MTR$_{asym}$ spectra of the substantia nigra, red nucleus, globus pallidus, putamen and caudate for all PD patients (n=27) and normal controls (n=22). The CEST effect was clearly visible in the offset range of 1–4 ppm in the MTR$_{asym}$ spectra. In regions of the substantia nigra and red nucleus, the CEST signal intensities were reduced in PD patients, compared to normal controls. Notably, the decreased MTR$_{asym}$ spectrum in the substantia nigra of PD patients appeared in a wide offset range, indicating a possible origin from cell loss that may cause the loss of all water-exchanging chemicals. In contrast, in regions of the globus pallidus, putamen and caudate, the CEST signal intensities were seemingly increased in PD patients, compared to normal controls. The maximal changes appeared at the offset of 3.5 ppm, where the amide protons of mobile proteins and peptides resonate.

Figure 2f quantitatively compares the average APT-weighted signal intensities of the substantia nigra, red nucleus, globus pallidus, putamen and caudate for all PD patients and normal controls. The MTR$_{asym}$(3.5 ppm) value of the substantia nigra was significantly lower in PD patients than in normal controls (1.0±0.2 % vs. 1.3±0.2 %, P=0.005). The MTR$_{asym}$(3.5 ppm) value of the red nucleus was also lower in PD patients than in normal controls, but the difference was not significant (1.0±0.2 % vs. 1.1±0.1 %, P=0.109). In contrast, the MTR$_{asym}$(3.5 ppm) values of the globus pallidus, putamen and caudate were significantly higher in PD patients than in normal controls (0.9±0.1 % vs. 0.5±0.2 %, $P<0.001$; 1.0±0.1 % vs. 0.8±0.2 %, P=0.003; 1.1±0.1 % vs. 0.7±0.2 %, $P<0.001$, respectively).

Two examples of the FLAIR images and APT-weighted images for a normal control and a PD patient are shown in Figs. 3 and 4. On the basis of Fig. 3, APT-weighted intensities in the basal ganglia were higher in PD patients than in normal controls. On the basis of Fig. 4, APT-weighted intensities in the midbrain were lower in PD patients than in normal controls.

Figure 5 compares the total CEST signal intensities of the substantia nigra, red nucleus, globus pallidus, putamen and caudate for all PD patients and normal controls. The total CEST signal intensity of the substantia nigra was significantly lower in PD patients than in normal controls (2.6±0.5 % vs. 3.6±0.4 %, P=0.006). The total CEST signal intensity of the red nucleus was also lower in PD patients than in normal
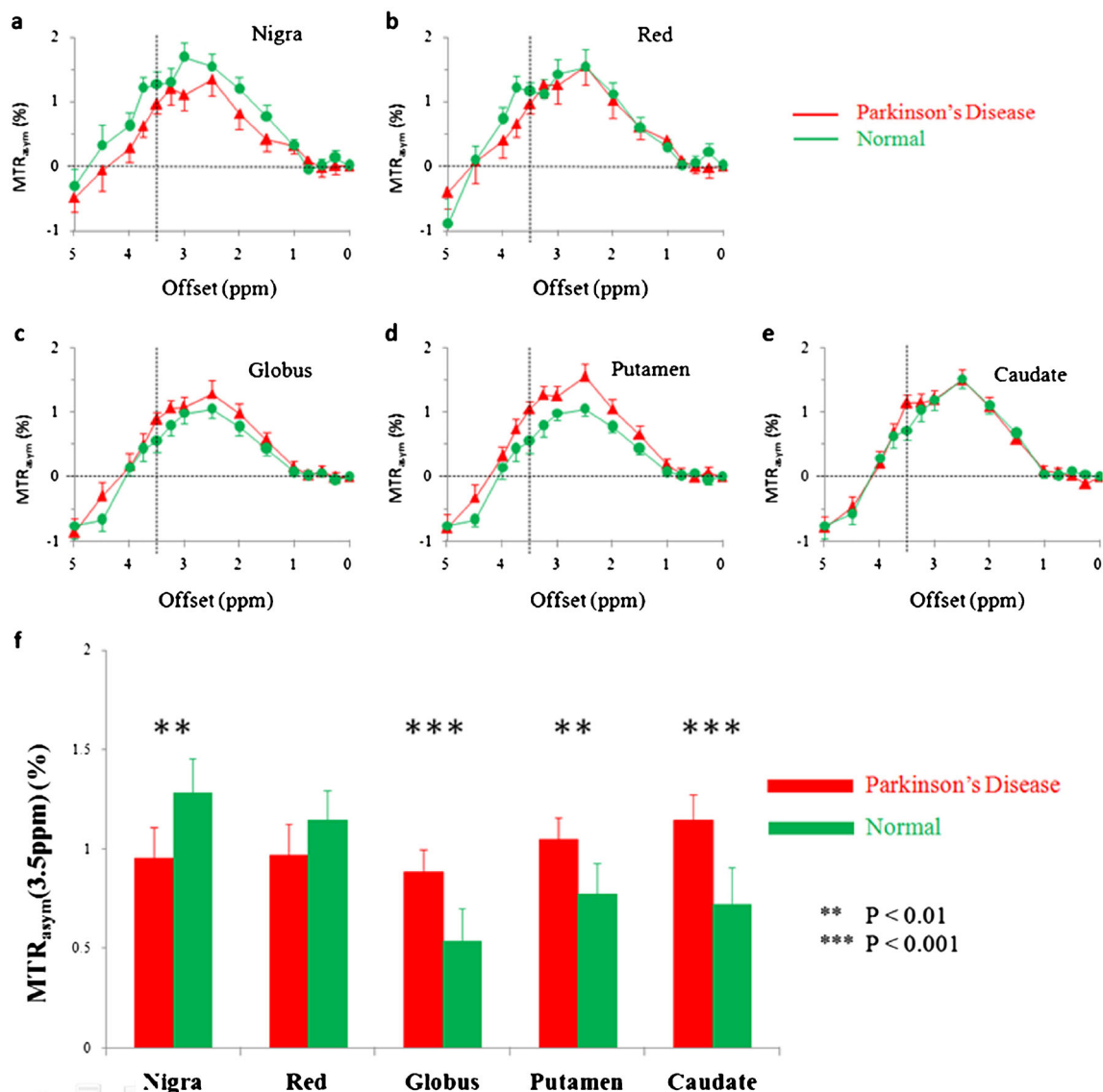
Fig. 2 Comparison of average MTR$_{asym}$ spectra of the substantia nigra, red nucleus, globus pallidus, putamen and caudate for Parkinson's disease (PD) patients ($n=27$) and normal controls ($n=22$). In regions of the substantia nigra (**a**) and red nucleus (**b**), the CEST effects were reduced in PD patients, compared to normal controls. In regions of the globus pallidus (**c**), putamen (**d**) and caudate (**e**), the CEST effects, particularly at the offset of 3.5 ppm, were increased in PD patients, compared to normal controls. The presence of the nuclear Overhauser enhancement effect in the brain upfield from the water resonance caused the negative CEST signals observed in the offset range >4.5 ppm in the MTR$_{asym}$ spectra for most brain regions [37, 38]. **f** Comparison of the corresponding average MTR$_{asym}$(3.5 ppm) signal intensities. ** $P<0.01$, *** $P<0.001$

controls (3.0 ± 0.6 % vs. 3.3 ± 0.5 %, $P=0.439$), but the difference was not significant. In contrast, the total CEST signal intensity of the globus pallidus was significantly higher in PD patients than in normal controls (2.5 ± 0.4 % vs. 2.0 ± 0.3 %, $P=0.029$). The total CEST signal intensities of the putamen and caudate were also higher in PD patients than in normal controls, but no significant differences were found (3.0 ± 0.3 % vs. 2.6 ± 0.3 %, $P=0.064$; 2.8 ± 0.3 % vs. 2.8 ± 0.2 %, $P=0.720$).

The results of MTR at the offset of 15.6 ppm are shown in Table 1. No significant differences in MTR(15.6 ppm) were found between PD patients and normal controls for these five regions.

The MTR$_{asym}$(3.5 ppm), MTR$_{asym}^{total}$ and MTR(15.6 ppm) values of the frontal NAWM and occipital NAWM are shown in Table 2. It is due to the presence of the confounding factors relating to MTR$_{asym}^{'}$ that the measured MTR$_{asym}$(3.5 ppm) values in the NAWM areas were negative [38]. No significant differences for these three parameters were found between PD patients and normal controls.

Characterization of the progression of PD

Table 3 compares the MTR$_{asym}$(3.5 ppm) values for all five regions for normal controls and for early-stage and advanced-

Fig. 3 **a** FLAIR image and **b** APT-weighted image of a typical normal control (female; 69 years old). **c** FLAIR image and **d** APT image of a PD patient (female; 76 years old; H&Y stage 1.5; unified Parkinson's disease rating scale 48). The CEST/APT imaging acquisition protocol provided B_0 inhomogeneity-corrected, APT-weighted images with sufficient signal-to-noise ratios. The APT-weighted intensities in regions of the basal ganglia (*white arrow*) were higher in PD patients than in normal controls. Note the presence of CSF artefacts (*black thin arrows*)
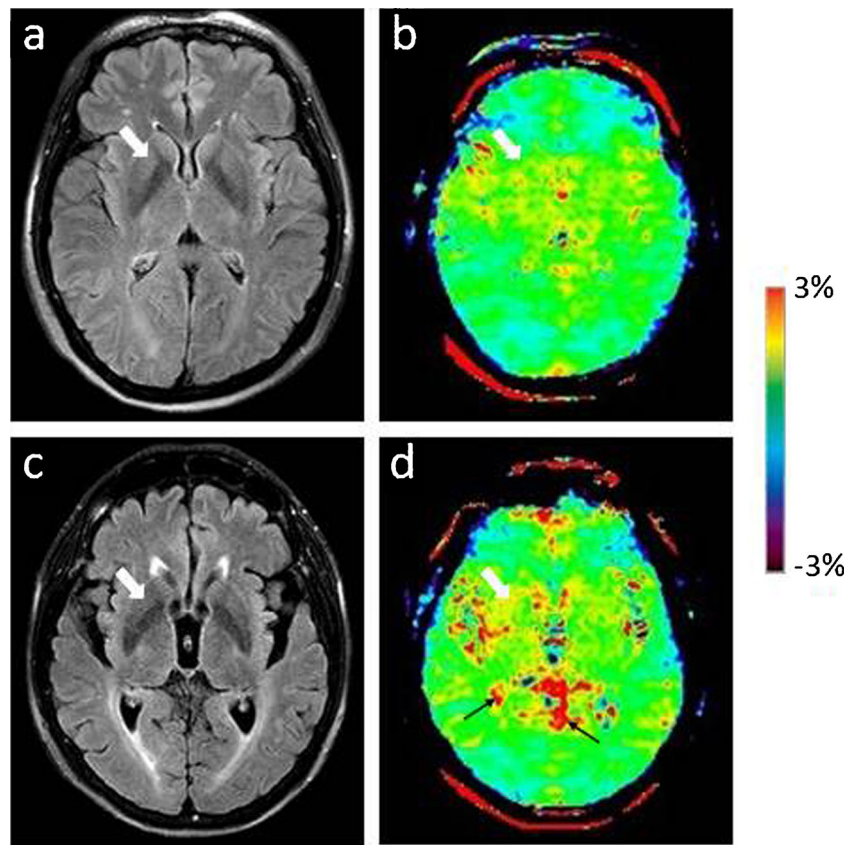

Fig. 4 **a** FLAIR image and **b** APT-weighted image of a typical normal control (female; 59 years old). **c** FLAIR image and **d** APT image of a PD patient (female; 61 years old; H&Y stage 1.5; unified Parkinson's disease rating scale 53). The APT-weighted intensities in regions of the midbrain (*white arrow*) were lower in PD patients than in normal controls. Note the presence of CSF artefacts (*black thin arrow*)
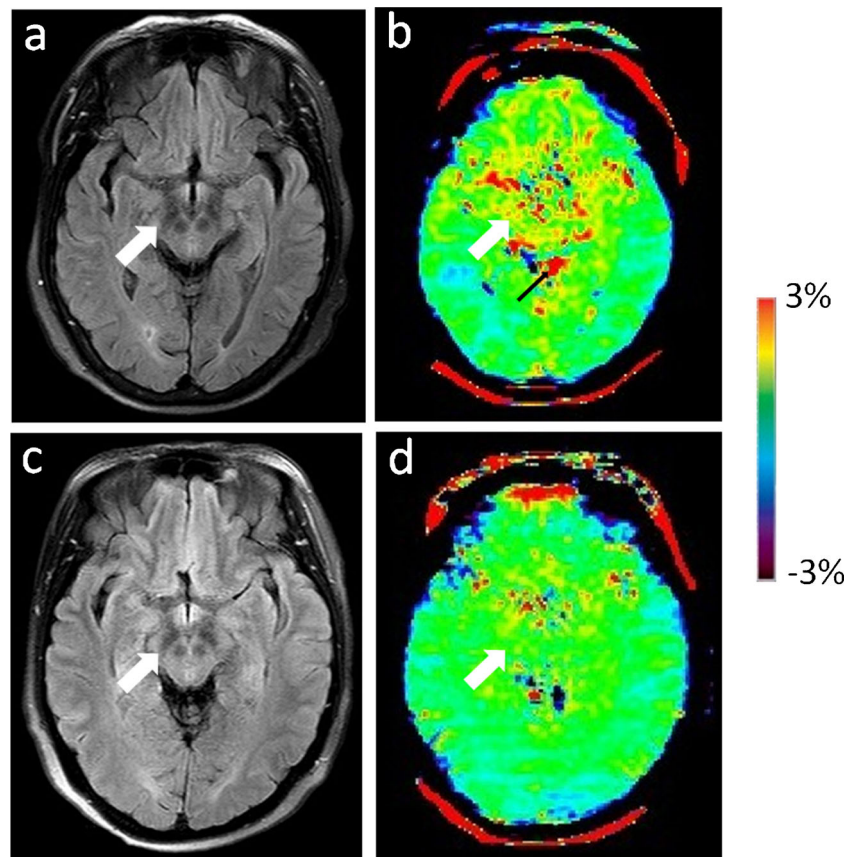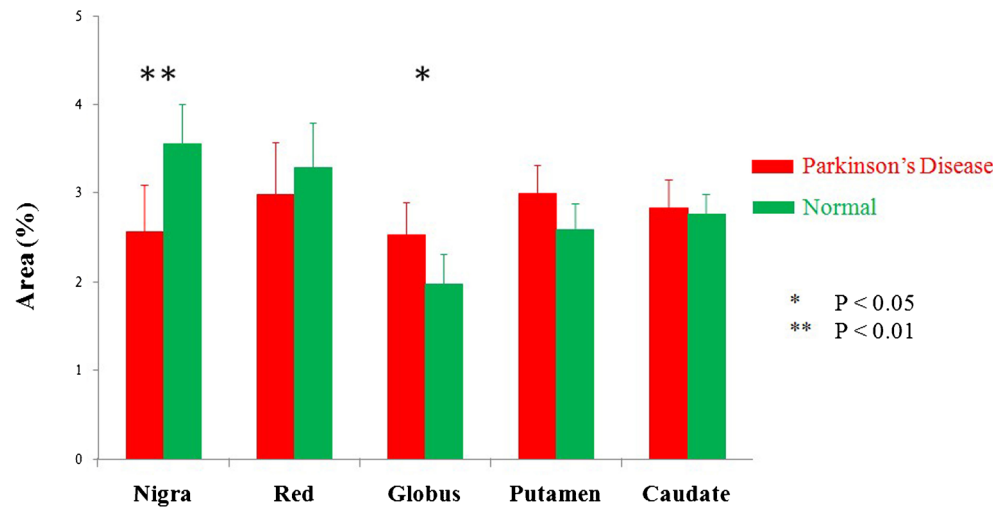
Fig. 5 Comparison of average total CEST signal intensities (integral of MTR_{asym} spectrum, MTR_{asym}^{total}) of the substantia nigra, red nucleus, globus pallidus, putamen and caudate for PD patients ($n=27$) and normal controls ($n=22$). * $P<0.05$, ** $P<0.01$

stage PD patients. It can be seen that the MTR_{asym}(3.5 ppm) intensities of the globus pallidus, putamen and caudate increased significantly from the normal controls to the early-stage PD. The results indicated that APT imaging may be used to differentiate PD patients, even at the early stage, from healthy people. Table 4 further compares the MTR_{asym}^{total} values for all five regions for normal controls, and early-stage and advanced-stage PD patients. It can be seen that the MTR_{asym}^{total} of the nigra substantia and red nucleus for PD patients showed a significant decrease from the early stage to the advanced stage. Therefore, CEST imaging may be used to characterize the progression of PD.

Discussion

PD is caused by the degeneration of the dopaminergic neurons in the substantia nigra and other brain structures [1]. It was reported previously that approximately 50 % of the dopaminergic cells of the substantia nigra are lost at the point of clinical expression of advanced-stage PD [32, 33]. The diagnosis of PD, especially at the early stage of this disease, remains challenging. Molecular pathology studies have shown that most neurodegenerative diseases are associated

with accumulations of abnormal proteins in the central nervous system [39, 40]. In PD, the pathological hallmarks are Lewy bodies and Lewy neuritis, in which the accumulated misfolded α-synuclein, a neuronal cytoplasmic protein, is the major component [34, 35]. These molecular results indicate the potential clinical utility of methods that can non-invasively visualize the protein content of PD in vivo.

CEST imaging is a novel molecular MRI technique that can detect endogenous, low-concentration chemicals in tissue non-invasively. The present study evaluated PD patients with CEST imaging for the first time. Our quantitative analysis focused on both the CEST signal at the offset of 3.5 ppm from water [MTR_{asym}(3.5 ppm)] and the total CEST signal (MTR_{asym}^{total}). MTR_{asym}(3.5 ppm) is more specific for quantifying the protein-based CEST effect at 3.5 ppm (i.e. APT for mobile proteins and peptides in tissue), while MTR_{asym}^{total} would better quantify CEST effects appearing at a wide offset range. We added the total CEST signal (MTR_{asym}^{total}) here because we wanted to find out the total tendency of MTR in PD patients. The preliminary results seem very promising. The fact that the MTR_{asym}(3.5 ppm) signal intensities of the globus pallidus, putamen and caudate were higher in PD patients than in normal controls (Fig. 2f) may be associated with increased cytosolic proteins and peptides, as expected [34, 35]. In contrast, the substantia nigra showed significantly lower total

Table 1 MTR(15.6 ppm) values (mean±95 % CI) for the substantia nigra, red nucleus, globus pallidus, putamen and caudate for PD patients ($n=27$) and normal controls ($n=22$)

	Substantia nigra	Red nucleus	Globus pallidus	Putamen	Caudate
PD	37.4±2.4	37.8±2.6	33.6±2.4	28.3±2.2	27.1±1.8
Normal	37.6±1.4	38.4±1.4	33.3±1.6	27.9±0.8	26.9±1.0
P value	0.514	0.159	0.495	0.179	0.465

MTR(15.6 ppm) was quantified by % water signal intensity

Table 2 MTR_{asym}(3.5 ppm), MTR_{asym}^{total} and MTR(15.6 ppm) values (mean±95 % CI) of the frontal NAWM and the occipital NAWM for PD patients (*n*=27) and normal controls (*n*=22)

	Frontal NAWM			Occipital NAWM		
	MTR_{asym}(3.5 ppm)	MTR_{asym}^{total}	MTR(15.6 ppm)	MTR_{asym}(3.5 ppm)	MTR_{asym}^{total}	MTR(15.6 ppm)
PD	−0.3±0.1	0.8±0.2	32.9±1.3	−0.1±0.1	1.0±0.2	31.0±0.8
Normal	−0.3±0.1	0.5±0.2	33.5±0.4	−0.1±0.1	1.0±0.1	31.5±0.7
P value	0.587	0.091	0.455	0.890	0.493	0.361

MTR_{asym}^{total} was defined as the integral of the MTR_{asym} spectrum in the range of 0 to 4 ppm. All were quantified by % water signal intensity

CEST signal intensities in PD patients than in normal controls (Fig. 5). Moreover, the decreased MTR_{asym} spectrum of the substantia nigra for PD patients appeared at a wide offset range (Fig. 2a). These results suggest that the changes could be attributed to the loss of dopaminergic neurons that may lead to the loss of all water-exchanging chemicals. The depletion of some chemicals with fast-exchanging protons, such as dopamine, may also reduce the whole MTR_{asym} spectrum as a result of the wide saturation width. However, the detection of the chemicals with fast-exchanging protons is not favourable at 3 Tesla. Therefore, the loss of dopaminergic neurons would be the more likely explanation for a decline in the whole MTR_{asym} spectrum.

The differences in MTR_{asym}(3.5 ppm) and MTR_{asym}^{total} among normal controls, early-stage PD patients and advanced-stage PD patients also seem quite important. The MTR_{asym}(3.5 ppm) and MTR_{asym}^{total} values decreased in all five regions of interest from the early stage to advanced stage of disease (Tables 3 and 4), although some changes did not reach significance. Notably, the MTR_{asym} and MTR_{asym}^{total} in the substantia nigra showed a consistently decreasing trend from normal controls to early-stage PD, to advanced-stage PD. This is consistent with the pathologic features of PD progression: a progressive neuronal loss in the nigrostriatal system and other neuronal networks. However, we also found that the MTR_{asym}(3.5 ppm) and MTR_{asym}^{total} values of the globus pallidus, putamen, caudate and even the red nucleus increased in PD patients at the early stage of disease, compared to normal controls, although these values seemed to decrease in the progression. Therefore, the MTR_{asym}(3.5 ppm) changes in these four regions were not simply monotonic during the progression of PD, which may be associated with medicine intervention. The exact mechanisms for these non-monotonic changes still require further study in the future.

Besides the five regions which are supposed to be related with PD, we also assessed two more regions which are probably not affected by PD, including the frontal NAWM and the occipital NAWM. This was done to confirm whether the effects of PD on the CEST/APT signals are specific for the five regions we focused on or can also be found in other brain regions. The results (Table 2) showed that the APT signals are stable in the NAWM in the different groups and confirmed the specificity of the observed CEST/APT findings for the five regions.

As a kind of neurodegenerative disease, PD demonstrated some potentially interesting CEST/APT image features in several regions of interest. Whether these findings are specific

Table 3 Measured MTR_{asym}(3.5 ppm) values (mean±95 % CI) for the substantia nigra, red nucleus, globus pallidus, putamen and caudate for normal controls and PD patients at different stages

	Normal (*n*=22)	Early stage PD (*n*=14)	Advanced stage PD (*n*=13)	*P* values
Substantia nigra	1.3±0.2	1.1±0.2	0.8±0.2	0.165, 0.061, 0.001*
Red nucleus	1.1±0.1	1.2±0.2	0.7±0.2	0.587, <0.001*, 0.001*
Globus pallidus	0.5±0.2	1.0±0.1	0.8±0.2	<0.001*, 0.238, 0.021*
Putamen	0.8±0.2	1.1±0.1	1.0±0.2	0.001*, 0.179, 0.087
Caudate	0.7±0.2	1.3±0.1	0.9±0.2	<0.001*, 0.003*, 0.113

MTR_{asym}(3.5 ppm) was quantified by % water signal intensity. The three *P* values correspond to results between normal controls and early-stage PD patients, between early-stage and advanced-stage PD patients, as well as between normal controls and advanced-stage PD patients, respectively

*Significant change

Table 4 Measured MTR_{asym}^{total} values (mean±95 % CI) for the substantia nigra, red nucleus, globus pallidus, putamen and caudate for normal controls and PD patients at different stages

	Normal (n=22)	Early stage PD (n=14)	Advanced stage PD (n=13)	P values
Substantia nigra	3.6±0.4	3.1±0.6	2.0±0.9	0.224, 0.030*, 0.001*
Red nucleus	3.3±0.5	3.7±0.8	2.3±0.8	0.431, 0.008*, 0.030*
Globus pallidus	2.0±0.3	2.6±0.6	2.4±0.5	0.028*, 0.490, 0.158
Putamen	2.6±0.3	3.1±0.4	2.9±0.5	0.044*, 0.392, 0.297
Caudate	2.8±0.2	3.0±0.4	2.7±0.5	0.323, 0.198, 0.648

MTR_{asym}^{total} was defined as the integral of the MTR_{asym} spectrum in the range of 0 to 4 ppm. The three P values correspond to the results between normal controls and early-stage PD patients, between early-stage and advanced-stage PD patients, as well as between normal controls and advanced-stage PD patients, respectively

*Significant change

for PD or common in other neurodegenerative diseases is also an important question. However, we suppose that these features may be specific for PD, because different neurodegenerative diseases have different pathogenesis and usually affect different brain regions. The exact results demand further studies on other kinds of neurodegenerative diseases.

Most previous studies [12–14] found that the MTR of the substantia nigra was lower in PD patients than in healthy people, and no differences were discovered in the globus pallidus, putamen or caudate. The MTR changes in the red nucleus seemed inconsistent on the basis of previous results. Both Tambasco et al. [12] and Anik et al. [13] found a lower MTR value in PD patients, while Morgen et al. [14] found no difference between PD patients and controls. However, we did not find any significant differences for the MTR(15.6 ppm) in any of the regions between normal controls and PD patients (Table 1), and this inconsistency may be due to the lower RF saturation power (2 μT) used in our protocol.

There were some limitations to this study. First, only two slices were obtained because of the limitation of the single-slice acquisition protocol. Thus, the MRI signal changes in other regions could not be evaluated in the present study. A novel, highly sensitive parallel transmission-based CEST technology, incorporated in the 3D imaging acquisition sequence [29], has been reported recently [41]. Second, it was a little difficult to select these five small regions exactly for the quantitative analysis, because of the limited resolution of CEST/APT imaging, even though we used FLAIR images as references. This may have influenced the accuracy of our results to some extent.

In conclusion, the CEST MRI methodology may be able to generate image contrasts that are based on the neuronal loss, as well as the changes in cytoplasmic proteins and peptides in several specific brain regions in PD patients. The CEST signals show great potential as imaging biomarkers that could detect disease and predict the progression. CEST MRI is a safe, completely non-invasive technology, and the results can be easily translated into the clinic for the molecular diagnosis of the disease.

References

1. Dauer W, Przedborski S (2003) Parkinson's disease: mechanisms and models. Neuron 39:889–909
2. Hughes AJ, Daniel SE, Kilford L, Lees AJ (1992) Accuracy of clinical diagnosis of idiopathic Parkinson's disease: a clinico-pathological study of 100 cases. J Neurol Neurosurg Psychiatry 55:181–184
3. Tolosa E, Wenning G, Poewe W (2006) The diagnosis of Parkinson's disease. Lancet Neurol 5:75–86
4. Michell AW, Lewis SJG, Foltynie T, Barker RA (2004) Biomarkers and Parkinson's disease. Brain 127:1693–1705
5. Seppi K, Poewe W (2010) Brain magnetic resonance imaging techniques in the diagnosis of parkinsonian syndromes. Neuroimaging Clin N Am 20:29–55
6. Vernon AC, Ballard C, Modo M (2010) Neuroimaging for Lewy body disease: is the in vivo molecular imaging of alpha-synuclein neuropathology required and feasible? Brain Res Rev 65:28–55
7. Schocke MFH, Seppi K, Esterhammer R et al (2002) Diffusion-weighted MRI differentiates the Parkinson variant of multiple system atrophy from PD. Neurology 58:575–580

8. Vaillancourt DE, Spraker MB, Prodoehl J et al (2009) High-resolution diffusion tensor imaging in the substantia nigra of de novo Parkinson disease. Neurology 72:1378–1384

9. Wang JJ, Lin WY, Lu CS et al (2011) Parkinson disease: diagnostic utility of diffusion kurtosis imaging. Radiology 261:210–217

10. Rossi M, Ruottinen H, Elovaara I et al (2010) Brain iron deposition and sequence characteristics in Parkinsonism comparison of SWI, T-2* Maps, T-2-weighted-, and FLAIR-SPACE. Investig Radiol 45: 795–802

11. Haller S, Badoud S, Nguyen D et al (2013) Differentiation between Parkinson disease and other forms of parkinsonism using support vector machine analysis of susceptibility-weighted imaging (SWI): initial results. Eur Radiol 23:12–19

12. Tambasco N, Pelliccioli GP, Chiarini P et al (2003) Magnetization transfer changes of grey and white matter in Parkinson's disease. Neuroradiology 45:224–230

13. Anik Y, Iseri P, Demirci A, Komsuoglu S, Inan N (2007) Magnetization transfer ratio in early period of Parkinson disease. Acad Radiol 14:189–192

14. Morgen K, Sammer G, Weber L et al (2011) Structural brain abnormalities in patients with Parkinson disease: a comparative voxel-based analysis using T1-weighted MR imaging and magnetization transfer imaging. Am J Neuroradiol 32:2080–2086

15. Zhou J, van Zijl PC (2006) Chemical exchange saturation transfer imaging and spectroscopy. Progr NMR Spectr 48:109–136

16. Vinogradov E, Sherry AD, Lenkinski RE (2013) CEST: from basic principles to applications, challenges and opportunities. J Magn Reson 229:155–172

17. Zhou J, Payen J, Wilson DA, Traystman RJ, van Zijl PCM (2003) Using the amide proton signals of intracellular proteins and peptides to detect pH effects in MRI. Nat Med 9:1085–1090

18. Zhou J, Tryggestad E, Wen Z et al (2011) Differentiation between glioma and radiation necrosis using molecular magnetic resonance imaging of endogenous proteins and peptides. Nat Med 17:130–134

19. van Buchem MA, Tofts PS (2000) Magnetization transfer imaging. Neuroimaging Clin N Am 10:771–788

20. Henkelman RM, Stanisz GJ, Graham SJ (2001) Magnetization transfer in MRI: a review. NMR Biomed 14:57–64

21. Cai KJ, Haris M, Singh A et al (2012) Magnetic resonance imaging of glutamate. Nat Med 18:302–306

22. Kogan F, Singh A, Debrosse C et al (2013) Imaging of glutamate in the spinal cord using GluCEST. NeuroImage 77:262–267

23. Chan KWY, McMahon MT, Kato Y et al (2012) Natural D-glucose as a biodegradable MRI contrast agent for detecting cancer. Magn Reson Med 68:1764–1773

24. Walker-Samuel S, Ramasawmy R, Torrealdea F et al (2013) In vivo imaging of glucose uptake and metabolism in tumors. Nat Med. doi: 10.1038/nm.3252

25. Ling W, Regatte RR, Navon G, Jerschow A (2008) Assessment of glycosaminoglycan concentration in vivo by chemical exchange-dependent saturation transfer (gagCEST). Proc Natl Acad Sci U S A 105:2266–2270

26. Jin T, Wang P, Zong XP, Kim SG (2012) Magnetic resonance imaging of the Amine-Proton EXchange (APEX) dependent contrast. NeuroImage 59:1218–1227

27. Jia G, Abaza R, Williams JD et al (2011) Amide proton transfer MR imaging of prostate cancer: a preliminary study. J Magn Reson Imaging 33:647–654

28. Dula AN, Arlinghaus LR, Dortch RD et al (2013) Amide proton transfer imaging of the breast at 3 T: establishing reproducibility and possible feasibility assessing chemotherapy response. Magn Reson Med 70:216–224

29. Zhou J, Zhu H, Lim M et al (2013) Three-dimensional amide proton transfer MR imaging of gliomas: initial experience and comparison with gadolinium enhancement. J Magn Reson Imaging 38:1119–1128

30. Sun PZ, Zhou J, Sun W, Huang J, van Zijl PCM (2007) Detection of the ischemic penumbra using pH-weighted MRI. J Cereb Blood Flow Metab 27:1129–1136

31. Zhao X, Wen Z, Huang F et al (2011) Saturation power dependence of amide proton transfer image contrasts in human brain tumors and strokes at 3 T. Magn Reson Med 66:1033–1041

32. Kirik D, Rosenblad C, Burer C et al (2002) Parkinson-like neurodegeneration induced by targeted overexpression of alpha-synuclein in the nigrostriatal system. J Neurosci 22:2780–2791

33. Hodaie M, Neimat JS, Lozano AM (2007) The dopaminergic nigrostriatal system and Parkinson's disease: molecular events in development, disease, and cell death, and new therapeutic strategies. Neurosurgery 60:17–28

34. Braak H, Sandmann-Keil D, Gai W, Braak E (1999) Extensive axonal Lewy neurites in Parkinson's disease: a novel pathological feature revealed by alpha-synuclein immunocytochemistry. Neurosci Lett 265:67–69

35. Tong JC, Wong H, Guttman M et al (2010) Brain alpha-synuclein accumulation in multiple system atrophy, Parkinson's disease and progressive supranuclear palsy: a comparative investigation. Brain 133:172–188

36. Wen Z, Hu S, Huang F et al (2010) MR imaging of high-grade brain tumors using endogenous protein and peptide-based contrast. NeuroImage 51:616–622

37. Zhou J, Blakeley JO, Hua J et al (2008) Practical data acquisition method for human brain tumor amide proton transfer (APT) imaging. Magn Reson Med 60:842–849

38. Zhou J, Hong X, Zhao X, Gao J-H, Yuan J (2013) APT-weighted and NOE-weighted image contrasts in glioma with different RF saturation powers based on magnetization transfer ratio asymmetry analyses. Magn Reson Med 70:320–327

39. Dawson TM, Dawson VL (2003) Molecular pathways of neurodegeneration in Parkinson's disease. Science 302:819–822

40. Peden AH, Ironside JW (2012) Molecular pathology in neurodegenerative diseases. Curr Drug Targets 13:1548–1559

41. Keupp J, Baltes C, Harvey PR, van den Brink J (2011) Parallel RF transmission based MRI technique for highly sensitive detection of amide proton transfer in the human brain. Proc 19th Annual Meeting ISMRM, Montreal, Quebec, p 710